DALTON
FULL PAPER

Patterns of hydrogen bonding in crystals of molybdenum carbonyl complexes †

Katja Heinze *

Anorganisch-Chemisches Institut der Universität Heidelberg, Im Neuenheimer Feld 270, 69120 Heidelberg, Germany. E-mail: katja.heinze@urz.uni-heidelberg.de

Received 19th July 2001, Accepted 14th November 2001
First published as an Advance Article on the web 29th January 2002

The solid-state structures of complexes of the type [HO–(N∩N′)]$Mo(CO)_3L$ (L = CO, THF, PPh_3, CN*t*Bu, CNCy) have been determined by X-ray crystallography. Two major types of multiple intermolecular hydrogen-bonding patterns involving the OH group and CH moieties as hydrogen donors and carbonyl groups and solvent molecules as hydrogen acceptors have been found and interpreted in terms of hydrogen bond strength, steric availability and dense packings. Discrimination between the two hydrogen-bonding patterns is also possible on the basis of unit cell dimensions and IR spectroscopy. DFT calculations support the interpretations.

Introduction

As a part of a program to synthesise inorganic and organometallic complexes on solid supports (solid-phase inorganic synthesis)[1,2] a number of molybdenum carbonyl complexes with a chelate ligand containing a pendant phenol group [HO–(N∩N′)] have been prepared and characterised.[1] It was anticipated that a variety of hydrogen-bonding patterns might be observed in the solid state due to the several possible hydrogen donor and hydrogen acceptor groups in different directions and the possibility of varying the co-ligand and adding external hydrogen acceptors. The understanding and control of the organisation of molecules—especially organometallic complexes—in the crystalline state has gained considerable interest as many properties of bulk materials, *e.g.* magnetism, conductivity, non-linear optical properties, *etc.*,[3] depend strongly on the crystal packing of the individual components. Hydrogen bonding has been of great importance in this context due to the relative strength and directionality of the bonds.[4] Most hydrogen bond research has been focused on the classical hydrogen bond donors and acceptors such as carboxylic acids, amides, halides and sulfides, resulting in strong hydrogen bonds, but it has also been recognised that C–H ··· O hydrogen bonds—albeit that they are weaker—play an important role.[5] Also, "non-conventional" hydrogen bonds occurring exclusively in organometallic compounds such as M ··· H–X, M–H ··· X and M–H ··· H–X have been reviewed recently.[5,6] The complexes described in the following are well suited for studying the interplay and competition between different types of hydrogen bonding, π–π interactions[7] and steric crowding occurring between the individual molecules in the solid state.

Results and discussion

Several molybdenum carbonyl complexes [HO–(N∩N′)]-$Mo(CO)_3L$ of the Schiff base chelate ligand with a pendant phenol group [HO–N∩N′)] (Scheme 1) were synthesised according to literature procedures[1] and their crystal structures determined.

† Electronic supplementary information (ESI) available: Fig. S1–S18 and Tables S1–S6 discussed in the text. See http://www.rsc.org/suppdata/dt/b1/b106456h/

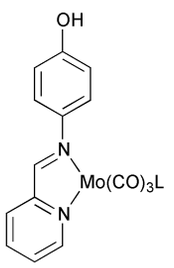

L	complex	model
CO	1	D-1
thf	2	D-2
PPh_3	3a•Et_2O	D-3; L = PH_3
PPh_3	3b	
CN*t*Bu	4	D-4; L = $CNCH_3$
CNCy	5	

Scheme 1 Complexes and model compounds.

Crystallographic studies

The molybdenum tetracarbonyl complex **1** (L = CO) crystallised from CH_2Cl_2 solutions layered with PE (bp 40–60 °C) as dark violet crystals in the centrosymmetric monoclinic space group $P2_1/c$. Selected bond lengths and angles are shown in Tables 1 and 2; the molecular structure of **1** is depicted in Fig. 1.

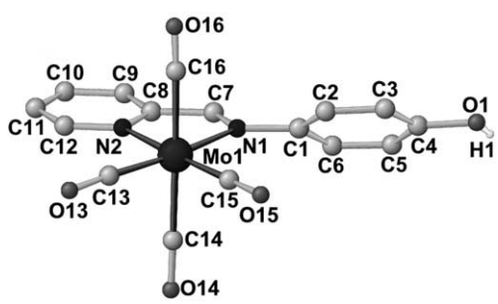

Fig. 1 Molecular structure of **1**.

The molecular geometry itself displays comparable features, *e.g.* to the related tetracarbonyl complex [R–(N∩N′)]-$Mo(CO)_4$,[8] so the discussion will be focused on the intermolecular interactions. This also applies to all following discussions.

Between individual molecules of **1**, C–H ··· OC contacts [5,9] are present (Fig. 2, Table 3). The hydrogen bonds C7–H7 ··· O13, C9–H9 ··· O13 and C5–H5 ··· O15 form C(6), C(7) and C(8) chains, respectively, in graph theory notation [10,11]. These connect molecules translated along the *a*-axis forming a triple hydrogen bond[12] of an AA ··· DDD type[13] (Scheme 2).

 DOI: 10.1039/b106456h

Table 1 Selected bond lengths (Å) for **1**–**5**

	1 (L = C16)	**2** (L = O16)	**3a** (L = P1)	**3b** (L = P1)	**4** (L = C16)	**5** (L = C16)
Mo1–N1	2.265(5)	2.254(4)	2.268(2)	2.276(2)	2.247(2)	2.270(1)
Mo1–N2	2.226(6)	2.275(4)	2.250(2)	2.262(2)	2.254(2)	2.253(1)
Mo1–C13	1.957(7)	1.943(5)	1.952(2)	1.946(2)	1.958(3)	1.959(2)
Mo1–C14	2.024(8)	1.922(5)	1.979(3)	1.974(3)	1.997(3)	2.003(2)
Mo1–C15	1.971(7)	1.942(5)	1.943(3)	1.930(2)	1.931(3)	1.935(2)
Mo1–L	2.072(8)	2.289(3)	2.5328(9)	2.5699(8)	2.166(3)	2.151(2)
C13–O13	1.161(8)	1.178(6)	1.165(3)	1.166(3)	1.159(3)	1.159(2)
C14–O14	1.148(8)	1.176(6)	1.149(3)	1.153(3)	1.148(3)	1.152(2)
C15–O15	1.163(8)	1.169(5)	1.172(3)	1.176(3)	1.180(3)	1.180(2)
N1–C7	1.291(8)	1.272(6)	1.301(3)	1.294(3)	1.290(3)	1.294(2)
N2–C8	1.361(8)	1.367(6)	1.360(3)	1.359(3)	1.362(3)	1.360(2)
C7–C8	1.456(9)	1.458(7)	1.449(4)	1.441(3)	1.443(4)	1.452(2)
N1–C1	1.440(8)	1.431(6)	1.428(3)	1.432(3)	1.434(3)	1.426(2)
O1–C4	1.377(8)	1.378(6)	1.374(3)	1.363(3)	1.369(3)	1.364(2)

Table 2 Selected bond angles (°) for **1**–**5**

	1 (L = C16)	**2** (L = O16)	**3a** (L = P1)	**3b** (L = P1)	**4** (L = C16)	**5** (L = C16)
N1–Mo1–N2	72.9(2)	72.4(1)	72.32(8)	71.99(7)	72.03(8)	72.05(5)
N1–Mo1–C13	167.4(2)	172.6(2)	171.06(9)	172.78(8)	168.20(9)	168.14(5)
N1–Mo1–C14	95.3(2)	101.9(2)	94.37(9)	95.12(9)	94.27(9)	98.34(6)
N1–Mo1–C15	101.3(2)	96.9(2)	101.65(9)	102.30(8)	103.88(9)	104.78(6)
N1–Mo1–L	90.7(2)	80.2(1)	92.25(6)	89.49(5)	82.82(9)	80.45(6)
N2–Mo1–C13	94.6(2)	103.4(2)	98.75(9)	100.91(9)	96.25(9)	96.92(6)
N2–Mo1–C14	93.2(2)	99.3(2)	95.4(1)	91.56(9)	88.22(9)	93.42(6)
N2–Mo1–C15	173.2(2)	168.8(2)	173.94(9)	174.14(8)	174.25(9)	176.75(5)
N2–Mo1–L	91.7(2)	77.7(1)	90.81(6)	89.43(5)	89.39(8)	84.40(5)
C13–Mo1–C14	83.6(3)	84.7(2)	85.9(1)	83.7(1)	86.6(1)	86.40(7)
C13–Mo1–C15	91.2(3)	86.9(2)	87.3(1)	84.77(9)	87.9(1)	86.19(6)
C13–Mo1–L	91.2(3)	93.0(2)	88.26(8)	91.71(8)	95.9(1)	94.43(7)
C14–Mo1–C15	85.6(3)	85.7(2)	85.5(1)	87.6(1)	88.1(1)	87.69(6)
C14–Mo1–L	173.2(3)	175.7(2)	172.04(8)	175.37(7)	176.7(1)	177.74(6)
C15–Mo1–L	90.1(3)	97.8(2)	88.80(8)	91.87(7)	94.1(1)	94.45(6)
C4–O1–H1 [C4A–O1A–H1XA]	106(8)	103(4)	110(8) [127(2)]	107(3)	111(2)	114(3)
O1–H1 ··· X [O100 ··· H1XA–O1A]	—	165(6)[a]	160(10)[b] [159(10)]	162(4)[c]	178(3)[c]	164(4)[c]
C7–N1–C1–C2	142.3(7)	−142.5(4)	145.5(3)	−141.9(2)	−138.6(2)	−144.8(2)
C7–C8–N2–C12	178.6(6)	−176.8(4)	−177.9(2)	−179.1(2)	178.8(2)	179.1(2)
Pyridine ··· C30–C35[d]	—	—	3.7/21	3.4/7	—	—
C1–C6 ··· C1A–C6A[d]	3.6/1	—	—	—	—	—

[a] X = O100. [b] X = O1(A). [c] X = O15(A). [d] Distance between ring centres (Å)/angle (°) between ring planes.

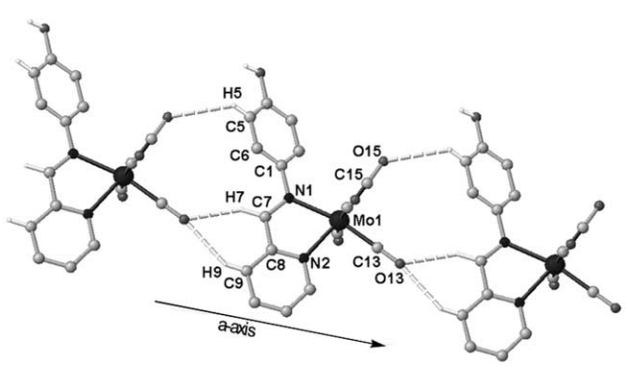

Fig. 2 Packing of **1** along the *a*-axis. Hydrogen bonds are indicated by dashed lines.

The chains are further bridged by single A ··· D hydrogen bonds, C2–H2 ··· O15 [C(7)], C5–H5 ··· O16 [C(8)] and C7–H7 ··· O1 [C(8)], in the *c*-direction (Tables 3 and S6, Fig. S1). Additionally, the chains are linked *via* face-to-face π–π interactions[7] of the phenol rings (C1–C6) along the *c*-axis (centroid–centroid distance 3.6 Å, angle between planes 1°, the rings stack in such a way that the N ⟶ O vectors of the substituents enclose an angle of 120°). The connection of

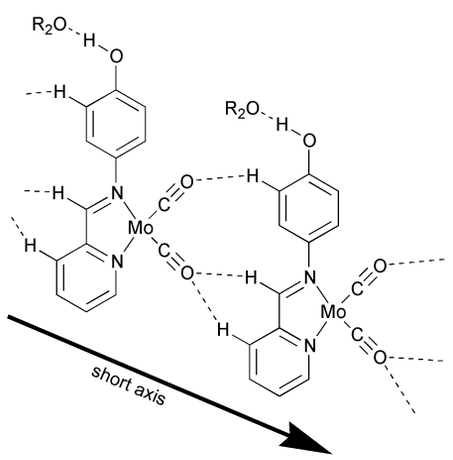

Scheme 2 Triple hydrogen-bonding system of the AA ··· DDD type. Axial ligands are omitted.

chains by hydrogen bonds and π–π interactions gives rise to a two-dimensional sheet structure (Fig. S1).

The tetrahydrofuran complex **2** (Fig. 3) crystallised from THF–PE in the monoclinic space group *I*2/*a* with additional

Table 3 Main geometrical parameters for H ··· O contacts and H ··· O interactions in complexes **1**, **2**, **3a**, **3b**, **4** and **5**[a]

	D	A	D–H	H ··· A	D–H–A	D ··· A	Motif	Atoms	Symmetry
1	C7–H7	O1	1.08	2.56	127.5	3.33	C(8)	O1–C4–C3–C2–C1–N1–C7–H7	Glide plane (c)
	C7–H7	O13	1.08	2.45	147.1	3.41	C(6)	O13–C13–Mo1–N1–C7–H7	Translation (a)
	C9–H9	O13	1.08	2.37	148.5	3.34	C(7)	O13–C13–Mo1–N2–C8–C9–H9	Translation (a)
	C2–H2	O15	1.08	2.55	145.7	3.50	C(7)	O15–C15–Mo1–N1–C1–C2–H2	Glide plane (c)
	C5–H5	O15	1.08	2.71	118.8	3.37	C(8)	O15–C15–Mo1–N1–C1–C6–C5–H5	Translation (a)
	C5–H5	O16	1.08	2.69	129.5	3.48	C(8)	O16–C16–Mo1–N1–C1–C6–C5–H5	Glide plane (c)
	C1–6	C1–6	—	—	1	3.60		π–π[b]	Glide plane (c)
2	O1–H1	O100(THF)	0.98	1.73	158.6	2.67	D	O100–H1–O1	—
	C7–H7	O13	1.08	2.93	101.9	3.32	C(6)	O13–C13–Mo1–N1–C7–H7	Translation (b)
	C9–H9	O13	1.08	2.86	105.4	3.31	C(7)	O13–C13–Mo1–N2–C8–C9–H9	Translation (b)
	C12–H12	O14	1.08	2.72	114.3	3.31	$R^2_2(12)$	O14–C14–Mo1–N2–C12–H12	Inversion
	C5–H5	O15	1.08	2.41	131.8	3.23	C(8)	O15–C15–Mo1–N1–C1–C6–C5–H5	Translation (b)
3a	O1–H1	O1	0.98	1.82	157.0	2.75	D	O1–H1–O1	Inversion
	O1–H1	O100(Et_2O)	0.98	1.63	159.9	2.57	D	O100–H1–O1	—
	C7–H7	O13	1.08	2.61	121.3	3.30	C(6)	O13–C13–Mo1–N1–C7–H7	Translation (a)
	C9–H9	O13	1.08	2.67	119.0	3.33	C(7)	O13–C13–Mo1–N2–C8–C9–H9	Translation (a)
	C43–H43	O13	1.08	2.59	150.9	3.57	C(9)	O13–C13–Mo1–P1–C40–C41–C42–C43–H43	2_1 (b)
	C44–H44	O14	1.08	2.54	141.7	3.45	C(8)	O14–C14–Mo1–P1–C40–C45–C44–H44	Glide plane (n)
	C9–H9	O14	1.08	2.58	155.6	3.59	$R^2_2(14)$	O14–C14–Mo1–N2–C8–C9–H9	Inversion
	C12–H12	O14	1.08	2.41	129.2	3.20	$R^2_2(12)$	O14–C14–Mo1–N2–C12–H12	Inversion
	C5–H5	O15	1.08	2.40	136.1	3.27	C(8)	O15–C15–Mo1–N1–C1–C6–C5–H5	Translation (a)
	C30–35	N2–C8–12	—	—	1	3.72		π–π[b] (intramolecular)	—
3b	C32–H32	O13	1.08	2.40	137.4	3.28	C(8)	O13–C13–Mo1–P1–C30–C31–C32–H32	2_1 (b)
	C33–H33	O13	1.08	2.70	138.1	3.58	C(9)	O13–C13–Mo1–P1–C30–C31–C32–C33–H33	Translation (b)
	C2–H2	O14	1.08	2.48	152.7	3.48	$R^2_2(14)$	O14–C14–Mo1–N1–C1–C2–H2	Inversion
	O1–H1	O15	0.98	1.87	157.6	2.80	C(10)	O15–C15–Mo1–N1–C1–C2–C3–C4–O1–H1	2_1 (b)
	C5–H5	O15	1.08	2.64	130.0	3.44	C(8)	O15–C15–Mo1–N1–C1–C6–C5–H5	2_1 (b)
	C34–H34	O15	1.08	2.47	149.2	3.44	C(8)	O15–C15–Mo1–P1–C30–C35–C34–H34	Translation (b)
	C30–35	N2–C8–12	—	—	7.5	3.40		π–π[b] (intramolecular)	—
	C20–25	C20–25	—	—	0	3.92		π–π[b]	Inversion
4	C12–H12	O1	1.08	2.50	121.2	3.20	C(10)	O1–C4–C3–C2–C1–N1–Mo1–N2–C12–H12	Translation (a)
	C11–H11	O13	1.08	2.41	129.6	3.21	C(7)	O13–C13–Mo1–N2–C12–C11–H11	2_1 (b)
	C5–H5	O14	1.08	2.68	118.6	3.33	C(8)	O14–C14–Mo1–N1–C1–C6–C5–H5	Glide plane (n)
	C3–H3	O15	1.08	2.63	130.8	3.43	$R^2_2(16)$	O15–C15–Mo1–N1–C1–C2–C3–H3	Inversion
	O1–H1	O15	0.98	1.84	168.6	2.81	$R^2_2(20)$	O15–C15–Mo1–N1–C1–C2–C3–C4–O1–H1	Inversion
5	C12–H12	O1	1.08	2.49	136.7	3.36	C(10)	O1–C4–C3–C2–C1–N1–Mo1–N2–C12–H12	Translation (a)
	C11–H11	O13	1.08	2.42	129.3	3.21	C(7)	O13–C13–Mo1–N2–C12–C11–H11	2_1 (b)
	C5–H5	O14	1.08	2.86	118.8	3.51	C(8)	O14–C14–Mo1–N1–C1–C6–C5–H5	Glide plane (n)
	C3–H3	O15	1.08	2.57	128.7	3.35	$R^2_2(16)$	O15–C15–Mo1–N1–C1–C2–C3–H3	Inversion
	O1–H1	O15	0.98	1.90	162.3	2.85	$R^2_2(20)$	O15–C15–Mo1–N1–C1–C2–C3–C4–O1–H1	Inversion

[a] The C–H and O–H distances are normalised (1.08 and 0.98 Å). The observed C–H and O–H distances are given in Table S6. All D ··· A distances < 3.6 Å and D–H ··· A angles > 115° (except for complex **2**) are reported. The full report of all contacts is for completeness only, with the aim of extracting common features. Not all contacts are necessarily considered attractive in nature, which might be particularly true for the CH ··· O contacts. [b] π–π interaction. Here the D ··· A distance corresponds to the distance between the ring centres and the D–H ··· A angle to the angle between the ring planes.

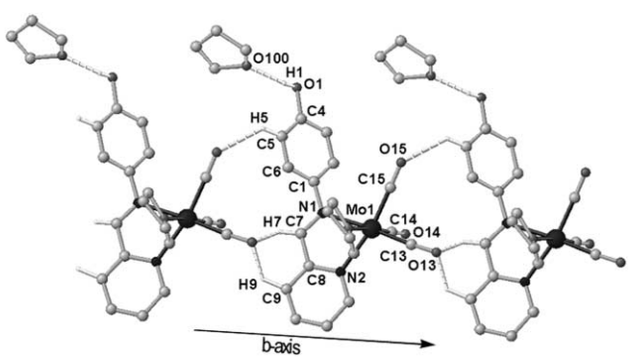

Fig. 3 Packing of **2** along the *b*-axis. Hydrogen bonds are indicated by dashed lines.

solvent molecules in the crystal lattice. One THF molecule is attached to the hydroxo group of the ligand *via* a hydrogen bond (Fig. 3, Table 3), with another THF molecule as a solvate (disordered and with s.o.f. < 1). Within graph theory description, the hydrogen-bonded aggregate is referred to as a finite D motif.[10] Two such solvent adducts are connected by a ring motif $R^2_2(12)$ [10,14] (Table 3, Fig. S2). The same combination of C(6), C(7) and C(8) chains, as found in the lattice of **1**, is present (although the C7–H7 ··· O13 and C9–H9 ··· O13 bonds are longer and more strongly bent than observed for compound **1**, Table 3) resulting in a triply linked chain (Scheme 2, Fig. 3). Together with a ring motif $R^2_2(12)$,[14] a one-dimensional band structure is obtained. These bands are blocked from further cross-linking due to the THF molecule blocking the OH group.[15]

A solvent-assisted hydrogen bond is observed in the solid-state structure of the triphenylphosphane complex **3a** as crystallised from CH_2Cl_2–Et_2O (Fig. 4). In this case, the OH group of the ligand acts both as a hydrogen donor and as a hydrogen acceptor (Table 3). Although disordered around a crystallographic inversion centre, this arrangement (including all hydrogen atoms) has been extracted from the diffraction

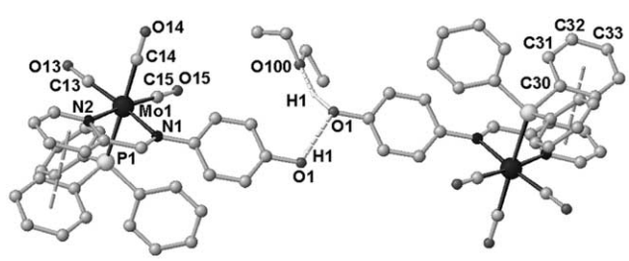

Fig. 4 Molecular structure of **3a**. Hydrogen bonds are indicated by dashed lines and π–π interactions by darker dashed lines.

data. Within graph theory, this aggregate is termed a finite DD structure.[10]

C–H ··· OC contacts between C7–H7 ··· O13 [C(6) motif], C9–H9 ··· 013 [C(7) motif] and C5–H5 ··· O15 [C(8) motif] of molecules translated along the *a*-axis are present giving the same triple hydrogen bonding of the AA ··· DDD type as found in the lattices of **1** and **2** (Fig. 5, Scheme 2, Table 3). Two

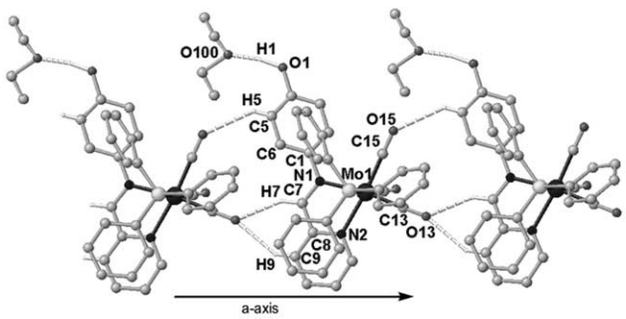

Fig. 5 Packing of **3a** along the *a*-axis. Hydrogen bonds are indicated by dashed lines.

further hydrogen bonds from CH groups of one phenyl ring of the phosphane ligand (C40–C45) to carbonyl groups of neighbouring molecules are present, connecting the triply linked chains in all directions (Tables 3 and S6, Fig. S3 and S4). In addition to these chain motifs, two ring motifs $R^2_2(12)$ and $R^2_2(14)$ (Tables 3 and S6, Fig. S5 and S6) are observed further cross-linking the molecules. The resulting structure has a three-dimensional architecture with all complexes nine-fold interconnected.[16]

If the same phosphane complex is crystallised from CH_2Cl_2–PE (in the absence of acceptor solvents), a completely different molecular packing is observed (a pseudo-polymorph[17,18]). The arrangement of the individual molecules of **3b** along the crystallographic *b*-axis is depicted in Fig. 6. Hydrogen bonds

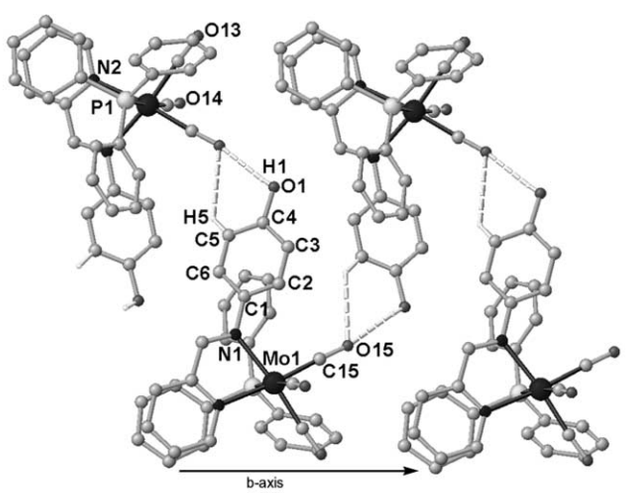

Fig. 6 Packing of **3b** along the *b*-axis. Hydrogen bonds are indicated by dashed lines.

from the OH group of the ligand to the carbonyl group (C15–O15)[19] *trans* to the pyridine of another molecule (related to the first by a two-fold screw axis) is observed (Fig. 6, Scheme 3 top/left, Table 3). This hydrogen-bonding pattern gives rise to a helical arrangement of the molecules along the crystallographic *b*-axis (2_1 screw axis) and can be described by a C(10) notation.[11] This rather strong hydrogen bond is accompanied by a weaker bond between O15 and H5 (Fig. 6: H5–C5–C6–C1–N1–Mo1–C15–O15; C(8) motif), resulting in a double hydrogen bond of the A ··· DD type (Scheme 3 top/left). This chain arrangement is similar to the catena motif found for carboxylic acids (Scheme 3 bottom/left). The helical chain is further stabilised by two single hydrogen bonds from phenyl hydrogen atoms (H33, H34) to carbonyl groups (O13, O15), giving a C(9) and a C(8) chain motif, respectively (Table 3, Fig. S7). Helices with different absolute configuration are linked in the *c*-direction *via* a C(8) motif of hydrogen bonds between C32–H32 ··· O13 and in the *a*-direction *via* a $R^2_2(14)$ ring motif of hydrogen bonds C2–H2 ··· O14 (Table 3, Fig. S8) propagated by a face-to-face π-stacking interaction[7] through one of the aromatic rings of the PPh_3 ligand (C20–C25; centroid–centroid distance 3.9 Å; the rings stack in such a way that the P ⟶ C vectors of the P substituent enclose an angle of 180°). Thus, a three-dimensional network is obtained with all complexes eight-fold connected.[20]

In addition to the intermolecular π–π interaction, an intramolecular contact between the pyridine ring of the ligand and one phenyl group of the phosphane ligand (C30–C35) with a centroid–centroid distance of 3.7 Å and an interplanar angle of 21° is observed,[7] as has also been found in the structure of **3a** (centroid–centroid distance 3.7 Å, interplanar angle 7°, Fig. 4).

The two isonitrile complexes **4** and **5** both crystallise from CH_2Cl_2–PE in the monoclinic space group $P2_1/n$ without solvent molecules. In both cases, a $R^2_2(20)$ ring motif (Fig. 7 and 8, Table 3) from the OH group of the ligand to the CO

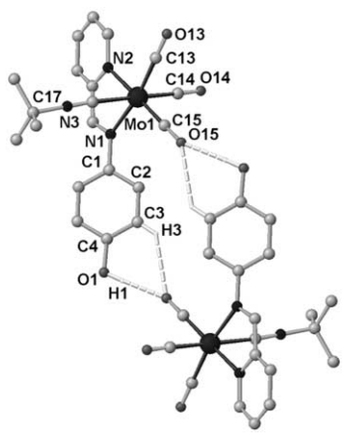

Fig. 7 Molecular structure of **4** showing the $R^2_2(20)$ and $R^2_2(16)$ motifs. Hydrogen bonds are indicated by dashed lines.

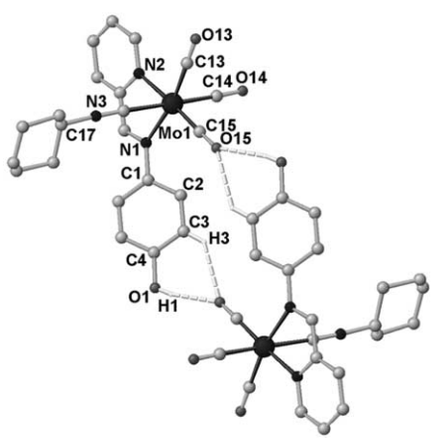

Fig. 8 Molecular structure of **5** showing the $R^2_2(20)$ and $R^2_2(16)$ motifs. Hydrogen bonds are indicated by dashed lines.

group (C15–O15) *trans* to the pyridine of the second complex is observed.[19] This strong hydrogen bond is assisted by a weak hydrogen bond between C3–H3 ··· O15 [ring motif $R^2_2(16)$], giving a double hydrogen bond of the A ··· DD type (Fig. 7 and 8, Scheme 3 top/right) similar to that found in the structure of **3b**. The motifs of **3a** and **3b** are thus similar concerning the local geometry but differ in the symmetry connecting the molecules: 2_1 screw axis for **3a** and inversion centre for **3b**,

Table 4 Experimental (CH_2Cl_2) and calculated (DFT) IR absorption energies and intensities and root-mean square deviation of experimental and DFT calculated geometries

	$\tilde{\nu}_{CO}$/cm^{-1} (intensity)	$\tilde{\nu}_{CN}$/cm^{-1} (intensity)	rms[a]/Å	Mulliken charges O13	O14	O15
1	2016 (m), 1910 (vs), 1889 (sh), 1839 (s)	—				
D-1	1965 (31), 1876 (35), 1872 (100), 1844 (60)		0.15	−0.19	−0.15	−0.18
2	1908 (vs), 1797 (br, vs)[b]	—				
D-2	1887 (100), 1813 (79), 1796 (86)		0.21	−0.22	−0.20	−0.21
3a/b	1919 (vs), 1827 (s), 1800 (s)	—				
D-3	1899 (100), 1831 (74), 1810 (89)		0.14	−0.21	−0.18	−0.21
4	1917 (vs), 1833 (s), 1803 (s)	2138 (s)				
D-4	1903 (100), 1845 (65), 1820 (79)	2176 (70)	0.20	−0.21	−0.18	−0.20
5	1918 (vs), 1834 (s), 1804 (s)	2132 (s)				
D-4	1903 (100), 1845 (65), 1820 (79)	2176 (70)	0.13			

[a] All ligand atoms (excluding H atoms) and the $Mo(CO)_3$ fragment were superimposed. [b] In THF.

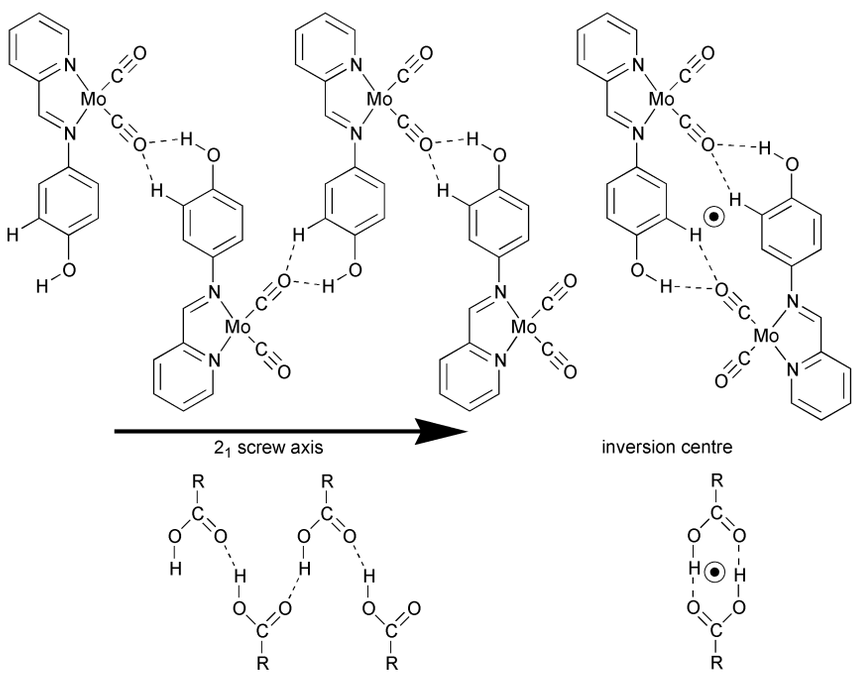

Scheme 3 Double hydrogen-bonding systems of the A ··· DD type around a 2_1 screw axis (left) and an inversion centre (right), and comparison with hydrogen bonding of carboxylic acids (bottom). Axial ligands are omitted.

which is topologically similar to the catena and ring motifs of carboxylic acids (Scheme 3 bottom).

Three chain motifs [C(7), C(8), C(10); Table 3] between hydrogen atoms of the ligand and carbonyl groups and the hydroxy oxygen are additionally observed in the solid-state structures of **4** and **5** (Fig. S9–S11). The combination of these hydrogen bonds results in a three-dimensional network structure with all complexes seven-fold connected.[21]

Computational studies and discussion

Individual complexes. To get further insight into the structure and bonding of the complexes, a DFT computational study was performed on all complexes or model complexes, respectively (Scheme 1). The geometries of the model complexes **D-1**–**D-4** (Scheme 1) were optimised and a frequency analysis was performed in each case. For all compounds, the calculated and experimental structures are in good agreement (Table 4, Fig. S12–S17).

As the phenolic hydroxo group and the phenol ring constitute very important sites for the intermolecular interactions, a closer inspection of these groups seems appropriate: for all compounds (and their models) the torsion angle C7–N1–C1–C2 of the phenol with respect to the imine is found to be around ±143(2) (experimental mean value) and ±138(2)° (calculated mean value). All other angular values found in the solid state are even more rigid (Table 2) and are also well reproduced by the DFT calculations (Tables S1–S4). Hence, the solid-state geometries of the individual molecules (excluding intermolecular interactions) are well described by the theoretical models, which is even true for the rather flexible phenol ring. This additionally shows that the orientation of the phenol ring is an intrinsic property of the molecules and not influenced by packing forces or hydrogen bonding. Furthermore, the IR data obtained experimentally in solution for the complexes **1**–**5**[1] and calculated by DFT methods for the model complexes **D-1**–**D-4** (frequencies are not scaled) agree well (Table 4). In summary, the DFT method is appropriate for modelling the structures of the individual complexes.

Hydrogen bonding of CH to CO. This type of hydrogen bonding is rather common in the crystal structures of organometallic compounds owing to the fact that a vast number of structures with carbonyl and CH-containing ligands exists. Usually, the donor–acceptor distances lie in the range 3.3 to 3.6 Å,[5] as has also been observed for complexes **1**–**5** (Table 3). A detailed metrical discussion of bond lengths and angles involving hydrogen atoms (although given for the sake of completeness in Table 3) is omitted due to the inherently poor accuracy of the hydrogen positions determined by X-ray crystallography. Remarkably,

hydrogen bonds in the crystal lattice of the tetracarbonyl complex **1** occur four times more often to carbonyl groups *trans* to nitrogen donors (O13, O15: 4 ×) than to the other CO groups (O14, O16: 1 ×). The former are supposed to be the most basic CO groups due to the stronger π-backbonding. This stronger basicity is also reflected in the computed Mulliken charges for the model complex **D-1** (Table 4). Replacing one CO ligand by weaker π-acceptors or stronger σ-donors in the complexes **2**–**5** renders the CO group *trans* to that ligand (C14–O14) more basic and thus allows for hydrogen bonding to that oxygen atom (Table 3). This explanation is in accord with the computed Mulliken charges of −0.18 to −0.21 for all the carbonyl oxygen atoms in the model complexes **D-2**–**D-4**.

Hydrogen bonding of OH to external acceptors. The experimental data show that hydrogen bonding to external hydrogen acceptors such as THF or Et_2O (**2**, **3a**) is favoured over hydrogen bonding of OH to the carbonyl groups of the $Mo(CO)_3$ fragment. The observation that CO participates in strong hydrogen bonding only when other (stronger) acceptors are not in competition has previously been made.[19]

Hydrogen bonding of OH to carbonyl groups. In the absence of external acceptors, the CO groups of the $Mo(CO)_3$ fragment become engaged in hydrogen bonding to the OH group (**3b**–**5**). There are only few precedents of such CO ··· HO interactions in the literature,[19,22] while CO ··· HC interactions are more common. In all cases, the CO ··· H angles are between 180 and 120° (**3b**: 167; **4**: 152; **5**: 150°) suggesting a ketone-like behaviour of the carbonyl groups.[6]

This is also reflected in the IR spectrum. The solid-state IR spectra of **3a** and **3b** are shown in Fig. 9.[23] A significant shift (24 cm^{-1}) of the band due to the asymmetric CO stretching vibration to lower energy is observed for the solvent-free complex **3b** as compared to that of **3a**. In the former case, the CO group (O15) is hydrogen bonded to a hydroxo group. In a qualitative MO description (although H-bonds are considered both electrostatic and covalent in nature), the donation of electrons occurs to some extent from the bonding π-orbital of the CO group (in addition to the σ* orbital) to the hydrogen atom, as suggested by the non-linear CO ··· H arrangement (Scheme 4). Thus, the C–O π-bonding orbital is depopulated, resulting in a weaker C–O bond strength and consequently leading to a low-energy IR absorption.

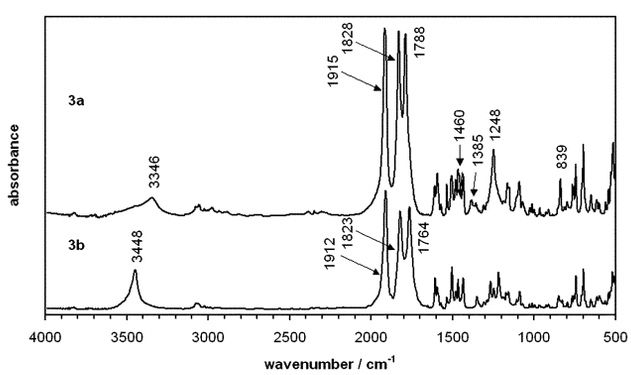

Fig. 9 IR spectra of **3a** and **3b** in CsI.

This interpretation is confirmed by a DFT calculation of the model complex **D-1** with a water molecule hydrogen-bonded to the appropriate CO group (**D-1·H_2O**, Scheme 4, Fig. S18, Table S5; O ··· H 1.96 Å, C–O ··· H 127°). The calculated shift of the absorption band due to the asymmetric CO stretching vibration is 28 cm^{-1}, in good agreement with the experimental value (Scheme 4).

The O ··· O distances between the acceptor and donor oxygen atoms are significantly shorter (**3b**: 2.80; **4**: 2.81; **5**: 2.85 Å) than those found in the solid-state structures of

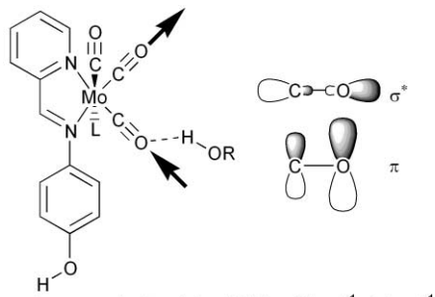

Scheme 4 Hydrogen bonding to carbonyl groups.

(η^6-2-methyl-1-hydroxyindenyl)$Cr(CO)_3$ (O ··· O 3.01 and 3.27 Å[19,22]) and $[(\mu\text{-}OH)_2\{(\eta^3\text{-}2\text{-}MeC_3H_4)(CO)_2\text{-}3,5\text{-}Me_2\text{-}pyrazole\}Mo_2]$ (O ··· O 3.00 and 2.95 Å[19,22]), suggesting a rather strong interaction. The O(carbonyl) ··· O(water) distance calculated for the model complex **D-1·H_2O** is 2.90 Å, in good agreement. Table 3 clearly shows that donor–acceptor distances for CH ··· OC interactions are greater than 3.0 Å, while the common "organic" hydrogen bonds between OH and hard acceptors such as solvent molecules show donor–acceptor distances less than 2.8 Å. Clearly, the observed distances for hydrogen bonds between OH and carbonyl groups in the structures of **3b**–**5** approach the values for the lengths of classical organic hydrogen bonds. This may be explained on the basis that the Schiff base ligand, as a rather strong donor, renders the molybdenum centre electron-rich and allows for strong π-backbonding to the CO groups. The carbonyl groups thus become rather electron-rich at the oxygen atoms.

The energetic difference between the chain motif C(10)/C(8) of **3b** and the ring motifs $R^2_2(20)/R^2_2(16)$ of **4** and **5** is probably not very large, as in both cases the same number and type of strong hydrogen bonds are present (Scheme 3 top; in the former case related by a screw axis and in the latter cases related by an inversion centre). The structures of the complexes **3b**–**5** therefore appear similar with respect to their strong hydrogen bonds, but differ concerning other weak interactions. In the phoshane complex **3b**, an additional π–π interaction exists between phosphane aryl rings of molecules belonging to different chains. This type of interaction would clearly be impossible in a ring motif, as the available phosphane aryl rings not involved in intramolecular π-stacking with the pyridine would be buried within the dimeric aggregate.

π–π interaction. π-stacking[7] is also relevant for complex **1**. Here, a π–π interaction between the phenol groups exists, in addition to weak CH ··· OC hydrogen bonds (Table 3). Such an interaction may be due to several reasons: the π-interaction is stronger than hydrogen bonding and/or the packing is more dense with stacked aromatic rings than with hydrogen bonds (increased packing efficiency). In this context, it is remarkable that with bulkier ligands than CO no π-stacking of phenol rings is observed, implying that there is too much steric crowding on one side of the phenol ring.

Common patterns. Although very different architectures (Table 5) are realised, two common hydrogen-bonding patterns are observed: the triple hydrogen bond (Scheme 2) and the double hydrogen bond (Scheme 3). Clearly, multiple hydrogen bonds have a larger predictive power due to their strength and their distinctive directionality in comparison to the weaker and more flexible single hydrogen bonds.[12] The investigated complexes can be divided into two groups (Table 5): **1**–**3a**, showing the triple hydrogen-bonding motif consisting of three weak

Table 5 Types of hydrogen-bonding motifs

	Short axis/Å	$\tilde{\nu}_{OH}$ [a]/cm^{-1}	OH group blocked by	Motif	Architecture [b]
1	9.056	3550	π–π interaction	AA ··· DDD chain	Sheet
2	7.905	3230	THF	AA ··· DDD chain	Band
3a	8.718	3346	Et_2O	AA ··· DDD chain	3D
3b	9.676	3448	—	A ··· DD chain	3D
4	11.576	3434	—	A ··· DD dimer	3D
5	11.537	3461	—	A ··· DD dimer	3D

[a] In CsI. [b] Including all hydrogen–acceptor contacts <3 Å and all π–π interactions.

CH ··· O bonds (AA ··· DDD type, Scheme 2) and **3b**–**5**, exhibiting the double hydrogen-bonding motif consisting of one rather strong OH ··· O and one weak CH ··· O bond (A ··· DD type, Scheme 3). For **2** and **3a**, formation of the double hydrogen bond is prevented by the solvent molecules blocking the hydroxo group, whereas for **1**, simultaneous π–π interaction between the phenol groups and engagement of the OH group in hydrogen bonding to a carbonyl group is sterically impossible (Table 5). Thus, it might be concluded that the double A ··· DD hydrogen bond is preferred, and only if this pattern cannot be formed is the triple AA ··· DDD pattern realised.

These different motifs are not only detected in the X-ray crystal structure determination, but also the cell parameters allow a differentiation to be made. Large cell axes prevent a translational packing, as required by the triple-bonding motif, while a short axis (approximately 8–9 Å) indicates this motif (Table 5). Additionally, IR spectroscopy allows a differentiation to be made: the frequency of the OH stretching vibration (Fig. 9, Table 5) obtained for complexes exhibiting the doubly bonding motif (**4b**–**6**) lie in a range of 3430–3460 cm^{-1}, while a hydrogen bond to a solvent molecule is indicated by frequencies below 3350 cm^{-1} (**3**, **4a**) and an almost undisturbed OH bond absorbs at frequencies above 3500 cm^{-1} (**1**). Thus, intermediate energies for the OH vibration indicate the double A ··· DD hydrogen bond motif.

Conclusion

It has been shown that several intermolecular interactions occur between complexes of the type [HO–N∩N′)]Mo(CO)$_3$L which determine the packing of the molecules. The balance and competition between these interactions (strong and weak hydrogen bonding, π–π stacking, packing efficiency) can not *a priori* be predicted in these structures, but can be explained in the context of strongest bonds/interactions, steric availability and dense packings. Two common hydrogen-bonding patterns have been discovered in the solid state structures of this type of complex. External hydrogen acceptors (solvent molecules) prevent formation of the double hydrogen-bonding motif A ··· DD and allow for the triple hydrogen-bonding pattern AA ··· DDD, so that in that respect, partial prediction and "design" of a crystal structure is possible. For the overall structure, all non-covalent interactions between the molecules have to be taken into account when trying to explain or, eventually, even predict crystal structures in the growing field of "inorganic crystal engineering".[3,4,6,15]

Experimental

Unless noted otherwise, all manipulations were carried out under argon by means of standard Schlenk techniques. All solvents were dried by standard methods and distilled under argon prior to use. All other reagents were used as received from commercial sources.

NMR: Bruker Avance DPX 200 at 200.15 (^{1}H) and 50.323 MHz (^{13}C) at 303 K; chemical shifts (δ) in ppm with respect to residual solvent peaks as internal standards: CD_2Cl_2 (^{1}H: δ = 5.32; ^{13}C: δ = 53.8). IR spectra were recorded on a BioRad Excalibur FTS 3000 spectrometer using CaF_2 cells or CsI disks. UV/Vis/NIR spectra were recorded on a Perkin Elmer Lambda 19 using 0.2 cm cells (Hellma, suprasil). FAB mass spectra were recorded on a Finnigan MAT 8400 spectrometer in 4-nitrobenzyl alcohol matrices. Elemental analyses were performed by the microanalytical laboratory of the Organic Chemistry Department, University of Heidelberg.

Computational method

Density functional calculations were carried out with the Gaussian98/DFT[24] series of programs. The B3LYP formulation of density functional theory was used, employing the LanL2DZ basis set.[24] Harmonic vibrational frequencies and infrared intensities were calculated by numerical second derivatives using analytically calculated first derivatives.

Crystallographic structure determinations

The measurements were carried out on an Enraf-Nonius Kappa CCD diffractometer using graphite monochromated Mo-Kα radiation. The data were processed using the standard Nonius software.[25] All calculations were performed using the SHELXT PLUS software package. Structures were solved using direct or Patterson methods with the SHELXS-97 program and refined with SHELXL-97.[26] Graphical handling of the structural data during refinement was performed using XMPA[27] and WinRay.[28] Atomic coordinates and anisotropic thermal parameters of the non-hydrogen atoms were refined by full-matrix least-squares calculations. Data relating to the structure determinations are collected in Table 6.

CCDC reference numbers 168307–168312.

See http://www.rsc.org/suppdata/dt/b1/b106456h/ for crystallographic data in CIF or other electronic format.

Synthesis

The synthesis of compounds **1**–**4** has been reported previously.[1] Complex **5** was prepared analogously to complex **4**, using 1 mmol cyclohexyl isonitrile instead of *tert*-butyl isonitrile (395 mg, 82%). Elemental analysis, found: C, 53.96; H, 4.44; N, 8.65%. $C_{22}H_{21}N_3O_4Mo$ requires C, 54.33; H, 4.34; N, 8.62%. *m*/*z* (FAB): 489 (M^+, 58), 461 ([M − CO]$^+$, 100). $\lambda_{max}(CH_2Cl_2)$ = 617 nm (6870 M^{-1} cm^{-1}). δ_H (CD_2Cl_2): 1.3–1.6 (m, 10 H, Cy-CH_2), 3.66 (s, br, 1 H, Cy-CH), 6.96 (br, d, 2H, *o*-CH), 7.41 (pt, 1H, Py-H^2), 7.48 (d, 2H, *m*-CH, $^3J_{HH}$ = 7 Hz), 7.87 (m, 2H, Py-H^3, Py-H^4), 8.55 (s, 1 H, N=CH), 9.22 (d, 1H, Py-H^1, $^3J_{HH}$ = 5 Hz). $\delta_C(CD_2Cl_2)$: 22.5, 25.3, 32.8 (s, Cy-CH_2), 116.0 (s, *o*-CH), 124.0 (s, *m*-CH), 125.8 (s, Py-C^2), 128.0 (s, Py-C^4), 136.3 (s, Py-C^3), 146.2 (s, *p*-C), 152.6 (s, Py-C^1), 155.1 (s, *i*-C), 157.0 (s, Py-C^5), 158.9 (s, N=CH), 210.2 (s, CO_{ax}), 227.4, 230.2 (s, CO_{eq}) [Cy-CH under solvent signal; CyN*C* not observed].

Crystals suitable for X-ray crystallographic determinations were obtained as follows: **2**: diffusion of PE into a THF solution; **3a**: diffusion of Et_2O into a CH_2Cl_2 solution; **1**, **3b**–**5**: diffusion of PE into CH_2Cl_2 solutions.

Table 6 X-Ray crystallographic data for **1**–**5**

	1	**2**	**3a**	**3b**	**4**	**5**
Formula	$C_{16}H_{10}N_2O_5Mo$	$C_{19}H_{18}N_2O_5Mo\cdot$ 0.95 THF	$C_{33}H_{25}N_2O_4PMo\cdot$ 0.5 Et_2O	$C_{33}H_{25}N_2O_4PMo$	$C_{20}H_{19}N_3O_4Mo$	$C_{22}H_{21}N_3O_4Mo$
Molecular mass	406.21	450.30	640.49	640.49	461.33	487.36
Crystal dimensions/mm	0.10 × 0.08 × 0.03	0.35 × 0.20 × 0.05	0.10 × 0.08 × 0.05	0.10 × 0.08 × 0.05	0.40 × 0.20 × 0.03	0.50 × 0.15 × 0.10
Crystal system	Monoclinic	Monoclinic	Monoclinic	Monoclinic	Monoclinic	Monoclinic
Space group (no.)	$P2_1/c$ (14)	$I2/a$ (15)	$P2_1/n$ (14)	$P2_1/n$ (14)	$P2_1/n$ (14)	$P2_1/n$ (14)
a/Å	9.056(2)	22.991(5)	8.718(2)	16.464(3)	11.576(2)	11.537(2)
b/Å	24.644(5)	7.905(2)	16.681(3)	9.676(2)	13.114(3)	12.954(3)
c/Å	7.091(1)	27.559(6)	21.761(4)	18.523(4)	13.293(3)	14.109(3)
β/°	108.93(3)	94.70(3)	95.32(3)	104.89(3)	92.89(3)	96.72(3)
Cell volume/Å^3	1497.0(5)	4992(2)	3151(1)	2852(1)	2015.4(7)	2094.1(7)
Molecular units per cell	4	8	4	4	4	4
μ/mm^{-1}	0.906	0.563	0.510	0.557	0.681	0.660
Density (calcd)/g cm^{-3}	1.802	1.381	1.418	1.492	1.520	1.546
T/K	200	200	200	200	200	200
Scan range (2θ/°)	4.8–60.1	4.8–55.7	4.5–64.1	3.8–64.1	4.4–60.0	4.3–74.0
Scan speed/sec frame^{-1}	10	20	10	10	5	5
Measured reflections	3781	22486	20837	19266	10509	19800
Unique reflections	2765	5935	10893	9904	5858	10629
Obs. reflections ($I \geq 2\sigma$)	1860	4072	7255	7035	4072	8333
Parameters refined	226	354	492	470	329	316
Max./min residual electron density/e Å^{-3}	1.55/−0.59	1.33/−0.55	1.24/−0.93	0.73/−0.99	0.76/−0.55	0.67/−1.297
Agreement factors (%)	$R_1 = 6.7$	$R_1 = 6.1$	$R_1 = 4.9$	$R_1 = 4.8$	$R_1 = 4.2$	$R_1 = 3.7$
F^2 refinement (%)	$R_w = 12.4$	$R_w = 18.4$	$R_w = 12.5$	$R_w = 13.1$	$R_w = 8.4$	$R_w = 10.1$

Acknowledgements

This work was supported by the Deutsche Forschungsgemeinschaft and the Fonds der Chemischen Industrie. The permanent, generous support of Prof. Dr. G. Huttner is gratefully acknowledged.

References and notes

1 K. Heinze, *Chem. Eur. J.*, 2001, **7**, 2922–2932.
2 K. Heinze, U. Winterhalter and T. Jannack, *Chem. Eur. J.*, 2000, **6**, 4203–4210.
3 D. Braga, *J. Chem. Soc., Dalton Trans.*, 2000, 3705–3713.
4 D. Braga and F. Grepioni, *Acc. Chem. Res.*, 1997, **33**, 601–608.
5 D. Braga, F. Grepioni, K. Biradha, V. R. Pedireddi and G. R. Desiraju, *J. Am. Chem. Soc.*, 1995, **117**, 3156–3166.
6 G. R. Desiraju, *J. Chem. Soc., Dalton Trans.*, 2000, 3745–3751.
7 C. Janiak, *J. Chem. Soc., Dalton Trans.*, 2000, 3885–3896.
8 E. C. Alyea, G. Ferguson and V. K. Jain, *Acta Crystallogr., Sect. C*, 1994, **50**, 854–857.
9 A. V. Malkov, I. R. Baxendale, M. Bella, V. Langer, J. Fawcett, D. R. Russell, D. J. Mansfield, M. Valko and P. Kočovský, *Organometallics*, 2001, **20**, 673–690.
10 J. Bernstein, R. E. Davis, L. Shimoni and N.-L. Chang, *Angew. Chem.*, 1995, **107**, 1689–1708; J. Bernstein, R. E. Davis, L. Shimoni and N.-L. Chang, *Angew. Chem., Int. Ed. Engl.*, 1995, **34**, 1555–1574.
11 C(n) denotes a chain with n atoms in the repeating unit.
12 For organic multiple hydrogen bonds, see: D. C. Sherrington and K. A. Taskinen, *Chem. Soc. Rev.*, 2001, **30**, 83–93.
13 This nomenclature summarises the sequence of hydrogen bond donor (D) and acceptor groups (A) on each of the interacting molecules.
14 $R^x_y(n)$: The superscript x denotes the number of hydrogen acceptors, the subscript y the number of hydrogen donors and n the ring size.
15 For an example of blocking strong hydrogen donor groups by solvent molecules, see: L. Brammer, J. C. M. Rivas, R. Atencio, S. Fang and F. C. Pigge, *J. Chem. Soc., Dalton Trans.*, 2000, 3855–3867.
16 The nine-fold connectivity is calculated as follows: 1 [D: O1H1 ··· O1] + 2 [C(6), C(7), C(8)] + 2 [C(9)] + 2 [C(8)] + 1 [$R^2_2(14)$] + 1 [$R^2_2(12)$] = 9.
17 D. Braga, G. Cojazzi, A. Abati, L. Maini, M. Polito, L. Scaccianoce and F. Grepioni, *J. Chem. Soc., Dalton Trans.*, 2000, 3969–3975.
18 D. Braga and F. Grepioni, *Chem. Soc. Rev.*, 2000, **29**, 229–238.
19 D. Braga, F. Grepioni and P. Sabatino, *Organometallics*, 1994, **13**, 3532–3543.
20 The eight-fold connectivity is calculated as follows: 2 [C(8), C(10)] + 2 [C(8), C(9)] + 2 [C(8)] + 2 [$R^2_2(20)$, π–π stacking] = 8.
21 The seven-fold connectivity is calculated as follows: 1 [$R^2_2(20)$, $R^2_2(16)$] + 2 [C(7)] + 2 [C(8)] + 2 [C(10)] = 7.
22 D. Braga and F. Grepioni, *Acc. Chem. Res.*, 1997, **30**, 81–87.
23 Absorption bands arising from the diethyl ether molecule in the crystal structure of **4a** are labelled in addition to the signals of OH and CO groups: 3020–2900 (CH_3, CH_2 stretching), 1460 (CH_2, deformation), 1385 (CH_3, deformation), 1248 cm^{-1} (C–O, stretching).
24 M. J. Frisch, G. W. Trucks, H. B. Schlegel, G. E. Scuseria, M. A. Robb, J. R. Cheeseman, V. G. Zakrzewski, J. A. Montgomery, Jr. R. E. Stratmann, J. C. Burant, S. Dapprich, J. M. Millam, A. D. Daniels, K. N. Kudin, M. C. Strain, O. Farkas, J. Tomasi, V. Barone, M. Cossi, R. Cammi, B. Mennucci, C. Pomelli, C. Adamo, S. Clifford, J. Ochterski, G. A. Petersson, P. Y. Ayala, Q. Cui, K. Morokuma, D. K. Malick, A. D. Rabuck, K. Raghavachari, J. B. Foresman, J. Cioslowski, J. V. Ortiz, B. B. Stefanov, G. Liu, A. Liashenko, P. Piskorz, I. Komaromi, R. Gomperts, R. L. Martin, D. J. Fox, T. Keith, M. A. Al-Laham, C. Y. Peng, A. Nanayakkara, C. Gonzalez, M. Challacombe, P. M. W. Gill, B. Johnson, W. Chen, M. W. Wong, J. L. Andres, C. Gonzalez, M. Head-Gordon, E. S. Replogle, J. A. Pople, Gaussian 98, revision A.6, Gaussian, Inc., Pittsburgh PA, 1998; http://www.gaussian.com.
25 R. Hooft, Collect, Data Collection Software, Nonius B. V., Delft, The Netherlands, 1998; http://www.nonius.com.
26 G. M. Sheldrick, SHELXS-97, Program for Crystal Structure Solution, University of Göttingen, Germany, 1997;; G. M. Sheldrick, SHELXL-97, Program for Crystal Structure Refinement, University of Göttingen, Germany, 1997; http://www.shelx.uni-ac.gwdg.de/shelx/index.html; *International Tables for X-ray Crystallography*, Kynoch Press, Birmingham, UK, 1974, vol. 4.
27 L. Zsolnai andG. Huttner, XPMA, University of Heidelberg, Germany, 1998; http://www.rzuser.uni-heidelberg.de/~ill/laszlo/xpm.html.
28 R. Soltek and G. Huttner, WinRay, University of Heidelberg, Germany, 1999; http://www.uni-heidelberg.de/institute/fak12/AC/huttner/frame/frame_soft.html.